

# Unified treatment of bound, scattering, and resonant states in one-dimensional semiconductor nanostructures

S. A. Rakityansky\*

*Physics Department, University of South Africa, P.O. Box 392, Pretoria 0003, South Africa*

(Received 25 April 2003; published 26 November 2003)

An exact and unified method is developed for finding a complete solution of the one-dimensional Schrödinger equation at any complex energy and for an arbitrary potential profile. This includes obtaining the binding energies, resonance energies and widths, transmission and reflection amplitudes, as well as the corresponding wave functions. In addition to finding the total widths of resonances, a simple but exact procedure is proposed for calculating their partial widths that determine relative probabilities of resonance decaying into (or exiting from) the left and right channels. The method is based on a direct calculation of the Jost matrix together with the Jost solutions of the Schrödinger equation. A combination of the variable-constant method with the complex coordinate rotation is used to replace this equation with an equivalent system of linear first-order differential equations whose solutions, taken at long distances from the interaction region, form the Jost matrix. The effectiveness and accuracy of the method are demonstrated by several numerical examples where the motion of particles through quantum-well semiconductor heterostructures as well as in a potential with infinite tails is considered.

DOI: 10.1103/PhysRevB.68.195320

PACS number(s): 73.63.-b, 73.23.-b

## I. INTRODUCTION

Thanks to advances in epitaxial growth technology, it has become possible in the last two decades to make crystal structures called superlattices, nanostructures, nanodevices, mesoscopic devices, and semiconductor heterostructures (see, for example, Ref. 1). These artificially grown crystals are composed of alternating layers of different semiconductor materials with nanometer thickness. The materials used in them have different energy gaps between the valence and conduction bands. As a result, for the electrons and holes, the layers represent a one-dimensional alternating sequence of potential wells and barriers.

By adjusting the chemical composition and thickness of the layers, it is possible, in principle, to construct a device with a given potential profile. This is why some authors (e.g., Ref. 2) use the term “wave function engineering” to emphasize the possibility of altering at will the shape of the wave function describing motion of the charge carriers in semiconductor devices, to suit specific applications.

The most ubiquitous example of a nanostructure is the sequence of GaAs and  $\text{Al}_x\text{Ga}_{1-x}\text{As}$  layers, where  $x$  is the aluminum mole fraction (usually  $x < 0.45$ ). When an electron moves through such a structure, it “feels” that inside the  $\text{Al}_x\text{Ga}_{1-x}\text{As}$  layers the potential energy is approximately  $944x$  meV higher than in the GaAs layers.<sup>3</sup> Therefore, for the electrons, the GaAs regions represent potential wells separated by the barriers that are formed by the  $\text{Al}_x\text{Ga}_{1-x}\text{As}$  layers. The GaAs/AlGaAs heterostructures are used in many electronic devices such as quantum-well infrared photodetectors,<sup>4</sup> tunneling diodes, and midinfrared lasers,<sup>5</sup> to name just a few.

The “wave function engineering” mentioned above, requires not only the sophisticated technology of crystal growing but also reliable methods for setting targets for such growing, i.e., methods for optimizing the potential profile

that generates desired spectrum of bound states and resonances of the charge carriers in the conduction band. There is a complicated technique of the inverse scattering problem that, in principle, enables one to reconstruct the potential profile from a given set of bound states and scattering characteristics.<sup>6</sup> In practice, however, the modeling is usually done by solving the direct problem, i.e., by locating the bound and resonant states for a given potential. In such an approach, the optimization is achieved by repeated solving of the direct problem for different potential profiles and choosing the optimal solution.

This “direct modeling” requires, of course, an efficient and accurate method for locating the bound states and resonances generated by one-dimensional potentials. Several methods of this kind have been developed over the past decades. Among them are the Numerov and finite element techniques, the transfer matrix and Green’s function approaches, the density of states, argument principle, perturbed wave vector, quantum reflection pole methods, and others (for references and review of the existing methods, see Ref. 7).

Bound states can be easily and accurately located by any of these methods, but when it comes to locating resonances, they show notable differences. By their approach to resonances, these methods can be divided into two categories that cover the real and complex energy calculations, respectively.

Using the real energy methods that are considered to be simple (although this is not always true), one can locate the position of relatively narrow resonances with a sufficiently high accuracy, but there are many difficulties in determining their widths and the methods usually fail for broad and overlapping resonances. The complex methods have the advantage that the calculations are based on a rigorous definition of resonances, namely, as singularities of the  $S$  matrix, and therefore the widths and resonant energies are obtained simultaneously.

Most of the existing real- as well as complex-energy

methods are based on discretization of the potential profile by a sequence of thin elements of rectangular shape with constant potential energy. For each of these elements, the wave function is a superposition of the right and left traveling plane waves. The superposition coefficients in two adjacent elements are related via the so-called transfer matrix that is constructed to satisfy the continuity condition. Then the total transfer matrix for the whole physical structure is a product of the elementary matrices.

Undoubtedly, the transfer-matrix approach is relatively simple and rather universal although it is not suitable in some cases. For example, it is difficult to use the transfer matrix when the potential has slowly decaying tails outside the physical structure (for instance, when charge is accumulated on the surfaces) and one has to go too far to achieve convergence of the results. The rectangular discretization is also not satisfactory when the potential profile has segments of fast variations (near impurities, for instance) or is biased by strong electric field<sup>8</sup> (Stark effect).

In the present work a method is developed for solving one-dimensional Schrödinger equation on an infinite line with an arbitrary potential profile. This method overcomes the abovementioned and some other drawbacks of the existing methods. It belongs to the category of complex-energy approaches and is based on exact differential equations that we derived (see Refs. 9–14) for functions closely related to the so-called Jost solutions well known in quantum scattering theory. At large distances these functions coincide with the elements of the Jost matrix. The zeros of the determinant of this matrix in the complex-energy plane correspond to the spectral points (bound and resonant states) of the Hamiltonian.

Unlike in the existing methods where the bound, scattering, and resonant states are treated differently, with the proposed equations one can obtain full solution of the problem for any chosen point in the complex-energy plane. In practical terms this means that with the same computer program that solves the same equations, one can obtain binding and resonant energies and widths as well as the transmission and reflection coefficients together with the corresponding wave functions by simply considering an appropriate domain of the complex-energy plane. A procedure is also developed for calculating the partial widths that determine relative probabilities that a resonance decays into (or excited from) the left and right moving waves (these probabilities are different when the potential is not symmetric).

The proposed method is simple in application and although it exploits the idea of the complex rotation of the coordinate (which is only needed for potentials with long tails), it is different than the traditionally used complex dilation methods (such as in Ref. 15, for example) in that it does not employ any expansion or variational procedures. Instead, the Jost matrix at a complex energy is obtained directly from exact equations equivalent to the effective-mass Schrödinger equation. The effectiveness and accuracy of the approach are demonstrated by several numerical examples where the motion of particles through quantum-well semiconductor heterostructures as well as in a potential with infinite tails is considered.

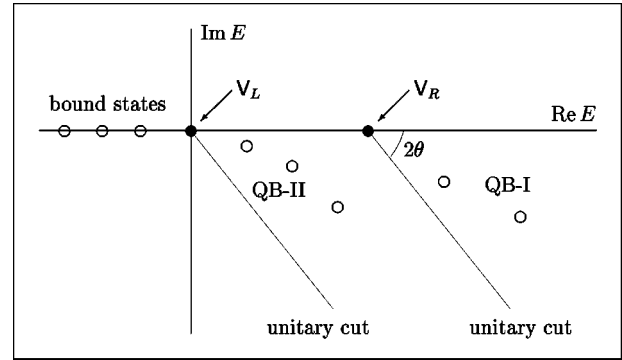


FIG. 1. Typical distribution of the bound states and resonances i.e. spectral points (open circles) in the complex energy plane. It is assumed that  $V_L < V_R$  and the energy is measured relative to  $V_L$ . The resonances that can decay in the both directions, are denoted as QB-I (quasibound states of the first type), and those that decay only to the left, as QB-II. The unitary cuts going from the branching points to infinity are also shown. Because of the complex rotation (33) these cuts are turned into the unphysical sheet by the angle  $2\theta$ .

## II. BASIC EQUATIONS

Consider a particle of mass  $m$  moving on the line  $x \in (-\infty, +\infty)$  where the potential energy  $V(x)$  becomes constant at both ends

$$V_{L-\infty \leftarrow x} V(x) \xrightarrow{x \rightarrow +\infty} V_R \quad (1)$$

faster than  $|x|^{-1}$ , i.e.,

$$\lim_{x \rightarrow \pm\infty} x[V(x) - V_{R,L}] = 0. \quad (2)$$

When  $V_L \neq V_R$  the potential  $V(x)$  is called biased. Without losing the generality, we can always assume that one of these limit values  $V_L$  or  $V_R$  (whichever is lower) is zero. This simply means that the energy is counted from this value and the bound states (if any) have negative energies as is usual when quantum mechanical systems are considered.

Wave function  $\Psi(E, x)$  describing the motion of this particle with the energy  $E$  obeys the Schrödinger equation

$$[\partial_x^2 + k^2 - V(x)]\Psi(E, x) = 0, \quad (3)$$

where

$$V(x) = \frac{2m}{\hbar^2} V(x)$$

and

$$k^2 = \frac{2m}{\hbar^2} E.$$

There are three different types of possible states of a quantum particle: bound, resonant, and scattering states. With the abovementioned choice of the origin of the energy scale, the corresponding wave functions are solutions of the same equation (3) at different complex  $E$ 's as shown in Fig. 1 and

with different boundary conditions.

For bound states the energy is real and negative while the wave function is square integrable. Corresponding solutions of Eq. (3), if they exist, have exponentially decaying asymptotic tails at the both ends of the  $x$  line

$$N_E^{(-)} e^{|k_L|x} \xleftarrow{-\infty \leftarrow x} \Psi(E, x) \xrightarrow{x \rightarrow +\infty} N_E^{(+)} e^{-|k_R|x}, \quad (4)$$

where

$$k_{L,R} = \sqrt{k^2 - V_{L,R}} \quad (5)$$

are the asymptotic values of the momentum (channel momenta) and  $N_E^{(\pm)}$  are the asymptotic normalization constants.

The resonances are described by the wave functions that have only outgoing waves at large distances

$$M_E^{(-)} e^{-ik_Lx} \xleftarrow{-\infty \leftarrow x} \Psi(E, x) \xrightarrow{x \rightarrow +\infty} M_E^{(+)} e^{ik_Rx}, \quad (6)$$

where  $M_E^{(\pm)}$  are also asymptotic normalization constants. The solutions of this kind exist at complex energies  $E = E_{\text{res}} - i\Gamma/2$  ( $E_{\text{res}} > 0$ ,  $\Gamma > 0$ ).

At this point it should be noted that the motion of a particle on an infinite line is inherently a multichannel problem that has at least two channels involved. These two channels are the motion on the left and right halves of the line. These channels open at the corresponding thresholds  $E = V_L$  and  $E = V_R$ . If the resonance energy  $E_{\text{res}}$  is above both these thresholds, the resonant state can decay into both channels (both directions), otherwise it can decay only into one of them.

Sometimes these two types of resonances are called quasisubbound states of the first and second type, respectively (see, for example, Ref. 7), although they have essentially the same nature since both correspond to the  $S$ -matrix poles in the complex energy plane. The boundary conditions are also the same, given by Eq. (6), for both ‘‘types’’ of resonances. Indeed, if, for example, the particle cannot go to  $-\infty$  (when the physical energy  $E_{\text{res}} < V_L$ ) then  $(k^2 - V_L) < 0$  and the left-moving plane wave  $\exp(-ik_Lx)$  in Eq. (6) automatically becomes exponentially attenuating, provided that, for a closed channel, we choose  $\text{Im} k_L > 0$  from the two possible signs when calculating the square root in Eq. (5).

When the potential is not symmetric and both channels are open, it is natural to expect that the probabilities of decaying of a resonance into (or its exciting from) the left and right channels may be different (as is usual in multichannel problems). The corresponding widths  $\Gamma_L$  and  $\Gamma_R$  in this case sum up to the total width  $\Gamma = \Gamma_L + \Gamma_R$ . In Appendix B, a procedure for determining the partial widths  $\Gamma_L$  and  $\Gamma_R$  is given.

The scattering happens at real positive energies. At large distances the corresponding wave function is a superposition of the incident and scattered waves, viz.

$$A(E) e^{ik_Lx} + A'(E) e^{-ik_Lx} \xleftarrow{-\infty \leftarrow x} \Psi(E, x) \xrightarrow{x \rightarrow +\infty} B'(E) e^{ik_Rx} + B(E) e^{-ik_Rx}, \quad (7)$$

where  $A$  and  $B$  are the amplitudes of the incoming waves (in the general case both  $A$  and  $B$  are nonzero, which means that the waves come from both the left and right channels) while  $A'$  and  $B'$  are the amplitudes of the scattered waves. When solving the scattering problems, we determine  $A'$  and  $B'$ .

As is seen, all these boundary conditions look quite different which necessitates the use of different mathematical methods for solving bound, resonance, and scattering problems. We can avoid this, however, if we find a convenient way to obtain the fundamental system of solutions of Eq. (3) at any complex  $E$ , and a unified way to construct the physical solutions obeying the boundary conditions (4), (6), and (7) out of it.

Since Eq. (3) is of the second order, its fundamental system of solutions consists of any two linearly independent functions obeying this equation (see, for example, Ref. 16). The choice of them is not unique like a choice of the basis in any space. To make our choice, we define two different solutions  $\phi_1(E, x)$  and  $\phi_2(E, x)$  of Eq. (3) by fixing values of them and their derivatives at  $x=0$  as follows:

$$\phi_1(E, 0) = 0, \quad \partial_x \phi_1(E, 0) = 1, \quad (8)$$

$$\phi_2(E, 0) = 1, \quad \partial_x \phi_2(E, 0) = 0. \quad (9)$$

Since the Wronskian of any two solutions of Eq. (3) is independent of  $x$ , we can calculate it at  $x=0$ . Hence

$$W(\phi_1, \phi_2) \equiv -1$$

for all points of the interval  $(-\infty, +\infty)$ , which means that the conditions (8) and (9) guarantee the linear independence of the solutions  $\phi_1$  and  $\phi_2$ . Hereafter they are called basic solutions.

At large distances the potential becomes constant and the general solution  $\Phi$  of Eq. (3) has the form

$$a(E) e^{ik_Lx} + a'(E) e^{-ik_Lx} \xleftarrow{-\infty \leftarrow x} \Phi(E, x) \xrightarrow{x \rightarrow +\infty} b'(E) e^{ik_Rx} + b(E) e^{-ik_Rx}, \quad (10)$$

similar to Eq. (7) with any choice of (complex)  $E$ . Any solution of Eq. (3) is a linear combination of its basic solutions  $\phi_1$  and  $\phi_2$ ,

$$\Phi(E, x) = C_1 \phi_1(E, x) + C_2 \phi_2(E, x).$$

Therefore, in constructing the physical solutions from the basic ones, we have to find such coefficients  $C_1$  and  $C_2$  that the asymptotics (10) takes the form of Eq. (4), (6), or (7). In order to facilitate this, we look for  $\phi_1$  and  $\phi_2$  in the following special form:

$$\phi_n(E, x) \equiv \begin{cases} e^{ik_Lx} F_{nL}^{(+)}(E, x) + e^{-ik_Lx} F_{nL}^{(-)}(E, x), & x \leq 0, \\ e^{ik_Rx} F_{nR}^{(+)}(E, x) + e^{-ik_Rx} F_{nR}^{(-)}(E, x), & x \geq 0, \quad n=1,2, \end{cases} \quad (11)$$

where  $F_{nL}^{(\pm)}(E, x)$  and  $F_{nR}^{(\pm)}(E, x)$  are new unknown functions. Since for each interval  $(-\infty, 0]$  and  $[0, +\infty)$  instead of one unknown function  $\phi_n$  (for each  $n$ ), we have introduced

two functions, they must be subjected to an additional constrain condition. The most convenient is the Lagrange condition

$$e^{ik_L x} \partial_x F_{nL}^{(+)}(E, x) + e^{-ik_L x} \partial_x F_{nL}^{(-)}(E, x) = 0, \quad x \leq 0,$$

$$e^{ik_R x} \partial_x F_{nR}^{(+)}(E, x) + e^{-ik_R x} \partial_x F_{nR}^{(-)}(E, x) = 0, \quad x \geq 0, \quad n = 1, 2, \quad (12)$$

which is standard in the variable-constant method for solving differential equations.<sup>17</sup>

Substituting the ansatz (11) into Eq. (3) and using the condition (12), we derive the following coupled differential equations of the first order:

$$\begin{aligned} \partial_x F_{nl}^{(+)}(E, x) &= \frac{e^{-ik_l x}}{2ik_l} [V(x) - V_l] [e^{ik_l x} F_{nl}^{(+)}(E, x) \\ &\quad + e^{-ik_l x} F_{nl}^{(-)}(E, x)], \\ \partial_x F_{nl}^{(-)}(E, x) &= -\frac{e^{ik_l x}}{2ik_l} [V(x) - V_l] [e^{ik_l x} F_{nl}^{(+)}(E, x) \\ &\quad + e^{-ik_l x} F_{nl}^{(-)}(E, x)], \end{aligned} \quad (13)$$

where the subscript  $l = L, R$  assumes the values  $L$  and  $R$  when  $x$  is on the left and right half lines  $x \in (-\infty, 0]$  and  $x \in [0, +\infty)$ , respectively.

To derive the boundary conditions for the functions  $F_{nl}^{(\pm)}$ , that correspond to the conditions (8), (9), we make use of Eqs. (11), (12) and obtain

$$\begin{aligned} F_{1l}^{(+)}(E, 0) + F_{1l}^{(-)}(E, 0) &= 0, \\ ik_l F_{1l}^{(+)}(E, 0) - ik_l F_{1l}^{(-)}(E, 0) &= 1 \end{aligned}$$

and

$$\begin{aligned} F_{2l}^{(+)}(E, 0) + F_{2l}^{(-)}(E, 0) &= 1, \\ ik_l F_{2l}^{(+)}(E, 0) - ik_l F_{2l}^{(-)}(E, 0) &= 0. \end{aligned}$$

Hence the boundary values of the functions  $F_{nl}^{(\pm)}$ , that guarantee the linear independence of the corresponding basic solutions  $\phi_n(E, x)$ , are ( $l = L, R$ )

$$F_{1l}^{(+)}(E, 0) = \frac{1}{2ik_l}, \quad F_{1l}^{(-)}(E, 0) = -\frac{1}{2ik_l}, \quad (14)$$

$$F_{2l}^{(+)}(E, 0) = \frac{1}{2}, \quad F_{2l}^{(-)}(E, 0) = \frac{1}{2}. \quad (15)$$

As can be easily checked, these conditions also guarantee the continuity of  $\phi_n(E, x)$  and its first derivative at  $x = 0$ . Equation (13) together with the boundary conditions (14), (15) define the fundamental system of solutions  $\phi_n(E, x)$  of Eq. (3) via Eq. (11). The functions  $F_{nl}^{(\pm)}(E, x)$  are closely related to the so-called Jost solutions well known in quantum scattering theory where they are defined as the solutions of the Schrödinger equation that at large distances converge to  $\exp(\pm ikr)$ .<sup>18</sup>

### III. JOST MATRIX AND $S$ MATRIX

Any physical solution  $\Psi(E, x)$  is a linear combination of the basic solutions

$$\Psi(E, x) = C_1 \phi_1(E, x) + C_2 \phi_2(E, x), \quad (16)$$

where the coefficients  $C_1$  and  $C_2$  are determined by the boundary conditions (4), (6), or (7) at large distances. To find appropriate coefficients in Eq. (16), we therefore need to know the behavior of  $\phi_1(E, x)$  and  $\phi_2(E, x)$  when  $x \rightarrow \pm \infty$ , which in turn requires the knowledge of the behavior of  $F_n^{(\pm)}(E, x)$  at the both ends of the interval  $(-\infty, +\infty)$  for various complex values of the energy  $E$ .

Comparing Eq. (11) with Eq. (10), we may expect that at large distances the functions  $F_{nl}^{(\pm)}(E, x)$  become constants. And indeed, if the difference  $[V(x) - V_l]$  vanishes fast enough when  $|x| \rightarrow \infty$  or becomes zero at finite  $|x|$ , then the right-hand sides of Eqs. (13) disappear, i.e.,

$$\partial_x F_{nl}^{(\pm)}(E, x) = 0, \quad |x| > x_{\max},$$

which means that  $F_{nl}^{(\pm)}(E, x) = \text{const}$  for large  $|x|$ .

In Appendix A it is shown that indeed, under the condition (2), in certain domains of the  $E$  plane these functions have finite limits  $F_{nl}^{(\pm)}(E, \pm \infty)$ . This question is discussed in Sec. IV, while here we describe how the physical solutions can be constructed if the necessary limiting values  $F_{nl}^{(\pm)}(E, \pm \infty)$  do exist. We show that these values can be combined in a  $2 \times 2$  matrix which has the same properties as the Jost matrix of the three-dimensional theory, namely, its zeros correspond to bound and resonant states, and it relates to the  $S$  matrix in the same way.

#### A. Bound states

When we use  $\phi_1(E, x)$  and  $\phi_2(E, x)$  to construct the wave function of a bound state, the coefficients  $C_1$  and  $C_2$  should be chosen in such a way that the resulting physical wave function  $\Psi(E, x)$  is exponentially decaying at large  $|x|$  in both directions as is given by Eq. (4). Of course, such a choice of  $C_1$  and  $C_2$  is possible only at certain points on the negative real axis of the  $E$  plane corresponding to the energies of bound states if they exist. Conversely, if we found a pair of numbers  $C_1$  and  $C_2$  such that the combination (16) obeys the conditions (4), then the energy at which this takes place is the bound state energy.

Substituting Eq. (11) into Eq. (16) we can rewrite the conditions (4) in terms of the functions  $F_{nl}^{(\pm)}(E, x)$  as follows:

$$C_1 F_{1L}^{(+)}(E, -\infty) + C_2 F_{2L}^{(+)}(E, -\infty) = 0,$$

$$C_1 F_{1R}^{(-)}(E, +\infty) + C_2 F_{2R}^{(-)}(E, +\infty) = 0. \quad (17)$$

This homogeneous system of linear algebraic equations for  $C_n$  has a nontrivial solution if and only if

$$\det \|f^{(-)}(E)\| = 0, \quad (18)$$

where the matrix  $\|f^{(-)}(E)\|$  is defined as

$$\|f^{(-)}(E)\| \equiv \lim_{x \rightarrow +\infty} \begin{pmatrix} F_{1L}^{(+)}(E, -x), & F_{2L}^{(+)}(E, -x) \\ F_{1R}^{(-)}(E, x), & F_{2R}^{(-)}(E, x) \end{pmatrix} \quad (19)$$

and by analogy with the standard three-dimensional scattering theory<sup>19</sup> can be called the Jost matrix.

So, the procedure of locating possible bound states is very simple. By solving the differential equations (13) from  $x = 0$  to certain  $|x_{\max}|$  in both directions, we calculate the matrix  $\|f^{(-)}(E)\|$  for different energies  $E$  on the negative real axis, trying to find such values among these energies at which Eq. (18) holds. This can take place at discrete points  $E_0, E_1, E_2, \dots$ , corresponding to the energies of bound states, if any. At each of the points  $E_i$  thus found, the coefficients  $C_1$  and  $C_2$  are then determined by the system (17) uniquely with the exception of the general normalization factor which is finally fixed when the physical wave function (16) is normalized.

### B. Resonances

Physical wave function of a resonance state, with asymptotic behavior given by Eq. (6), can be constructed out of the basic solutions just in the same way as for bound states. As is easily seen, the conditions (6) give the same homogeneous linear equations (17) for the coefficients  $C_1$  and  $C_2$ . Therefore the resonance energies  $E_{\text{res}}$  and the total widths  $\Gamma$  are also determined by roots  $E_r$  of Eq. (18). The only difference is that the resonance zeros of Eq. (18) are complex and the channel momenta (5) should be taken on the physical ( $\text{Im } k_i > 0$ ) or unphysical ( $\text{Im } k_i < 0$ ) sheet of the Riemann surface (see Appendix A) if the corresponding channel is closed or open. This choice between the physical and unphysical sheets is dictated by the necessity to obey the boundary conditions, i.e., to have attenuating or growing waves at large distances. Since the resonances in the open channels are only possible at positive collision energies  $E_{\text{res}}$ , the corresponding zeros  $E_r$  are situated below the positive real axis of the complex  $E$  plane

$$E_r = E_{\text{res}} - \frac{i}{2}\Gamma.$$

Locating complex zero  $E_r$  of the Jost matrix, we determine both the energy and total width of a resonance at the same time. A procedure for calculating the partial widths  $\Gamma_L$  and  $\Gamma_R$  is given in Appendix B.

Therefore the positions of both bound and resonant states are given by zeros of the determinant of the same matrix (19). This is yet another reason why we call it the Jost matrix.

### C. Scattering states

Quantum scattering is a transformation of the incoming waves into outgoing waves at real positive energies (when  $E$  is above at least one of the limit values  $V_L$  and  $V_R$ ) by the effect of the potential, which can be schematically presented as follows:

$$\begin{array}{ccc} \Psi_{\text{in}} : & \begin{array}{c} A(E)e^{ik_L x} \\ \wedge \wedge \wedge \wedge \longrightarrow \end{array} & \begin{array}{c} \boxed{V} \\ \longleftarrow \wedge \wedge \wedge \wedge \\ B(E)e^{-ik_R x} \end{array} \\ & & \Downarrow \\ \Psi_{\text{out}} : & \begin{array}{c} A'(E)e^{-ik_L x} \\ \longleftarrow \wedge \wedge \wedge \wedge \end{array} & \begin{array}{c} B'(E)e^{ik_R x} \\ \wedge \wedge \wedge \wedge \longrightarrow \end{array} \end{array}$$

Here we consider the general case when the incident waves come from the both sides with the left and right amplitudes being  $A(E)$  and  $B(E)$ , respectively. After the interaction has taken place the scattered waves also diverge in both directions. Each of the scattered waves  $A'(E)e^{-ik_L x}$  and  $B'(E)e^{ik_R x}$  include the corresponding transmitted and reflected waves. The waves that span to the far left ( $-\infty$ ) and far right ( $+\infty$ ) ends of the  $x$  line can be considered as moving in two different channels ( $L$  and  $R$  channels, respectively) coupled by the potential. If  $E$  is above both  $V_L$  and  $V_R$ , both channels are open and the waves can be transmitted between them. Otherwise only reflection (elastic scattering) in the open channel is possible.

Since the flux of the particles is conserving we have

$$|A(E)|^2 + |B(E)|^2 = |A'(E)|^2 + |B'(E)|^2,$$

which implies that the incoming wave amplitudes are transformed into the outgoing ones by a unitary  $2 \times 2$  matrix

$$\begin{pmatrix} A' \\ B' \end{pmatrix} = S \begin{pmatrix} A \\ B \end{pmatrix}. \quad (20)$$

Matrix elements of the  $S$  matrix can be obtained as a by-product when we construct the physical wave function. Indeed, substituting Eqs. (16) and (11) into Eq. (7), we obtain two systems of linear equations involving the coefficients  $C_n$ , viz.

$$\begin{aligned} C_1 F_{1L}^{(+)}(E, -\infty) + C_2 F_{2L}^{(+)}(E, -\infty) &= A, \\ C_1 F_{1R}^{(-)}(E, +\infty) + C_2 F_{2R}^{(-)}(E, +\infty) &= B, \end{aligned} \quad (21)$$

$$\begin{aligned} C_1 F_{1L}^{(-)}(E, -\infty) + C_2 F_{2L}^{(-)}(E, -\infty) &= A', \\ C_1 F_{1R}^{(+)}(E, +\infty) + C_2 F_{2R}^{(+)}(E, +\infty) &= B'. \end{aligned} \quad (22)$$

At first sight, it seems that we have too many equations for  $C_1$  and  $C_2$ . Since, however,  $A$  and  $B$  are given amplitudes of the incident waves while  $A'$  and  $B'$  are unknown quantities, we have four unknowns here. The coefficients  $C_1$  and  $C_2$  should be obtained from the system (21). Then the scattered wave amplitudes  $A'$  and  $B'$  can be calculated by means of Eqs. (22).

Equations (21) and (22) can be rewritten in the matrix form

$$\|f^{(-)}(E)\| \begin{pmatrix} C_1 \\ C_2 \end{pmatrix} = \begin{pmatrix} A \\ B \end{pmatrix} \quad \text{and} \quad \begin{pmatrix} A' \\ B' \end{pmatrix} = \|f^{(+)}(E)\| \begin{pmatrix} C_1 \\ C_2 \end{pmatrix}, \quad (23)$$

where the matrix  $\|f^{(-)}(E)\|$  is defined by Eq. (19) while  $\|f^{(+)}(E)\|$  is

$$\|f^{(+)}(E)\| \equiv \lim_{x \rightarrow +\infty} \begin{pmatrix} F_{1L}^{(-)}(E, -x), & F_{2L}^{(-)}(E, -x) \\ F_{1R}^{(+)}(E, x), & F_{2R}^{(+)}(E, x) \end{pmatrix}. \quad (24)$$

The scattering wave function normalized to the incoming flux  $|A|^2 + |B|^2$  is therefore given by the following product of row,  $2 \times 2$ , and column matrices

$$\Psi^{\text{scatt}}(E, x) = \begin{pmatrix} e^{ik_l x} F_{1l}^{(+)}(E, x) + e^{-ik_l x} F_{1l}^{(-)}(E, x) \\ e^{ik_l x} F_{2l}^{(+)}(E, x) + e^{-ik_l x} F_{2l}^{(-)}(E, x) \end{pmatrix}^T \times \|f^{(-)}(E)\|^{-1} \begin{pmatrix} A \\ B \end{pmatrix},$$

where  $l=L$  for negative  $x$  and  $l=R$  for  $x>0$ .

Comparing Eqs. (23) with the definition of the  $S$  matrix (20), we see that

$$S(E) = \|f^{(+)}(E)\| \|f^{(-)}(E)\|^{-1}. \quad (25)$$

This equation has exactly the same form as the expression of the  $S$  matrix in terms of the Jost matrix and its conjugate partner, which is introduced in the three-dimensional theory of multichannel and noncentral potentials.<sup>18,19,13</sup> It should also be noted that at the spectral points (bound and resonant states) where the condition (18) holds, the matrix (25) has poles, as one would expect from an  $S$  matrix.

The matrix elements of the  $S$  matrix do not depend on the choice of the initial wave amplitudes  $A$  and  $B$ . Therefore to clarify the physical meaning of these matrix elements we can consider special cases with simple choices of  $A$  and  $B$ .

If  $A \neq 0$  and  $B = 0$  (left incoming wave) then  $R_L = A'/A$  and  $T_L = B'/A$  are the left reflection and transmission amplitudes, respectively. Similarly, if  $A = 0$  and  $B \neq 0$  then  $R_R = B'/B$  and  $T_R = A'/B$  are the right reflection and transmission amplitudes. Substituting  $A = 0$  or  $B = 0$  into the equation

$$\begin{pmatrix} A' \\ B' \end{pmatrix} = \begin{pmatrix} S_{11}A + S_{12}B \\ S_{21}A + S_{22}B \end{pmatrix}$$

we see that the  $S$  matrix consists of these transmission and reflection amplitudes, namely,

$$S(E) = \begin{pmatrix} R_L(E), & T_R(E) \\ T_L(E), & R_R(E) \end{pmatrix}. \quad (26)$$

It should be noted that in the above equation,  $E$  is complex and only for real energies the quantities  $R_l$  and  $T_l$  have the simple physical meaning. If  $E$  is real, one can prove the following relations between them (see, for example, Ref. 20). When the interaction is time-reversal invariant the left and right transmission amplitudes are equal,  $T_L = T_R$ . Furthermore, in this case, the left and right reflection coefficients coincide as well,  $|R_L|^2 = |R_R|^2$ , which follows from the fact that the total current is conserving, i.e.,  $|T_l|^2 + |R_l|^2 = 1$ .

Therefore, when an appropriate domain of the complex-energy plane is considered, the differential equations (13) together with boundary conditions (14), (15) at  $x=0$ , give full solution of the one-dimensional problem for bound, scat-

tering, and resonant states in a unified way. For any complex  $E$ , by solving these equations from  $x=0$  to  $|x_{\text{max}}|$ , one obtains not only the Jost and  $S$  matrices but at the same time the functions  $F_{nl}^{(\pm)}(E, x)$  that give the corresponding physical wave functions, via Eqs. (11) and (16), with guaranteed correct behavior at large distances.

In many practical problems concerning the semiconductor heterostructures, the potential is constant for all  $x$  outside certain finite interval  $|x| < x_{\text{max}}$ . In such cases the limits

$$F_{nl}^{(\pm)}(E, \pm\infty) = F_{nl}^{(\pm)}(E, \pm x_{\text{max}})$$

apparently exist for any complex  $E$ , and therefore Eqs. (13) can be applied as they are, without any of the modifications (complex rotation) discussed in the subsequent sections. In general, however,  $V(x)$  can be of the long-range nature if, for example, electric charge is accumulated at the surfaces of the heterostructure.<sup>3,21</sup> Such problems can also be solved using the proposed method, though a more careful analysis (see Appendix A) shows that, for locating resonances, they require a different path (along a line in the complex  $x$  plane) for integration of Eqs. (13).

#### IV. LONG-RANGE BEHAVIOR OF $F^{(\pm)}$

As is shown in Appendix A, in the general case of a long-range potential obeying the constraint (2), the functions  $F_{nl}^{(+)}(E, x)$  and  $F_{nl}^{(-)}(E, x)$  have finite limits ( $|x| \rightarrow \infty$ ) in different domains of the Riemann  $E$  surface, namely, in the domains defined by

$$F_{nl}^{(-)}(E, x) \xrightarrow{|x| \rightarrow \infty} (\lim \exists \text{ if } \text{Im } k_l x \geq 0), \quad (27)$$

$$F_{nl}^{(+)}(E, x) \xrightarrow{|x| \rightarrow \infty} (\lim \exists \text{ if } \text{Im } k_l x \leq 0), \quad (28)$$

where  $x \rightarrow -\infty$  for  $l=L$  and  $x \rightarrow +\infty$  for  $l=R$ . In other words

$$\begin{aligned} (\lim \exists \text{ if } \text{Im } k_L \leq 0) &\xleftarrow{-\infty \leftarrow x} F_{nl}^{(-)}(E, x) \\ &\xrightarrow{x \rightarrow +\infty} (\lim \exists \text{ if } \text{Im } k_R \geq 0), \end{aligned} \quad (29)$$

$$\begin{aligned} (\lim \exists \text{ if } \text{Im } k_L \geq 0) &\xleftarrow{-\infty \leftarrow x} F_{nl}^{(+)}(E, x) \\ &\xrightarrow{x \rightarrow +\infty} (\lim \exists \text{ if } \text{Im } k_R \leq 0). \end{aligned} \quad (30)$$

Comparing these conditions with the definitions (19) and (24) of the Jost matrix and its conjugate partner, we see that the matrices  $\|f^{(-)}(E)\|$  and  $\|f^{(+)}(E)\|$ , exist in the following domains of the  $E$  surface:

$$\|f^{(-)}(E)\| \exists \text{ if } \text{Im } k_l \geq 0, \quad (31)$$

$$\|f^{(+)}(E)\| \exists \text{ if } \text{Im } k_l \leq 0. \quad (32)$$

They exist simultaneously only on the real axis of the  $E$  plane. For different limits, this axis serves therefore as either the lower or upper bound of the corresponding domains of the  $E$  plane. Such an ultimate separation of the upper and lower half planes takes place, however, only for long-range

potentials. If the potential decays very fast (exponentially, for instance) the lower bound is shifted downwards and the upper bound upwards which results in a widening of the common domain of the  $E$  plane. That is, for short-range potentials all the above limits exist simultaneously when  $E$  is within a band along the real axis (see Appendix A).

The fact that  $F_{nl}^{(\pm)}(E, x)$  has no limits in certain domains of the  $E$  plane seems to contradict the asymptotics (10) that are valid for any complex  $E$ . These asymptotics, however, are written in a general form and must include both terms involving  $\exp(ik_l x)$  and  $\exp(-ik_l x)$ , only if  $\text{Im } k_l x = 0$ , when they are of the same order of magnitude. If  $\text{Im } k_l x \neq 0$ , then one of the exponential functions  $\exp(\pm ik_l x)$  is growing while the other is vanishing. This means that in such a case the left- and right-hand sides of Eq. (10) are sums of “small” and “large” terms. The “small” term is significant only at the spectral points where the “large” term is zero by definition. At all other points and off the real axis, the asymptotics (10) does not prescribe the structure of any “small” terms, and therefore we should keep only the leading terms at the left and right hand sides of Eq. (10). If either  $F_{nl}^{(+)}(E, x)$  or  $F_{nl}^{(-)}(E, x)$  diverges, it is always multiplied in Eq. (11) by a vanishing exponential function that compensates its growth so that the corresponding term does not contribute into the leading order asymptotic behavior of the function (11) and therefore does not contradict Eq. (10).

Thus, the two-term decomposition (11) guarantees term by term correspondence with the asymptotic form (10) when  $\text{Im } k_l x = 0$  and at the spectral points (bound and resonant states). For the other points of the  $E$  plane, one of the terms (11) at large distances acquires a diverging admixture which, however, remains infinitesimal compared to the other term that corresponds to the leading term of the asymptotics (10).

Since the limits of  $F_{nl}^{(\pm)}$  do not exist for all complex  $E$ 's the applicability of Eqs. (13) generally (in the case of long-range potentials) is limited, namely, using these equations we can solve only the scattering problem ( $S$  matrix for real  $E$ ) and locate bound states (zeros of the Jost matrix  $||f^{(-)}(E)||$  on the negative real axis). In the resonance domain of the  $E$  plane (under the real axis) Eqs. (13) generally do not give us  $||f^{(-)}(E)||$  since the required limits  $\lim_{x \rightarrow +\infty} F_{nl}^{(-)}(E, x)$  do not exist. This difficulty, however, can be circumvented by using a complex integration path which is discussed next.

## V. COMPLEX ROTATION

The conditions (28) and (27) for the existence of the long-range limits of the functions  $F_{nl}^{(\pm)}(E, x)$  involve the imaginary part of the product  $k_l x$  but not of the momentum alone. This offers an elegant way to extend the domains of the  $E$  plane where these limits exist, to practically the whole  $E$  plane. Indeed, if, for example,  $\text{Im } k_l x$  is negative we can always make it positive by using complex values of  $x$ .

Let us assume that the long-range tail of  $V(x)$  is an analytic function of  $x$ . Suppose it grows faster than  $|x|^{-1}$  at both ends of the line (see Fig. 2)

$$x = z \exp(i\theta), \quad \text{Im } z = 0, \quad z \in [-\infty, +\infty], \quad (33)$$

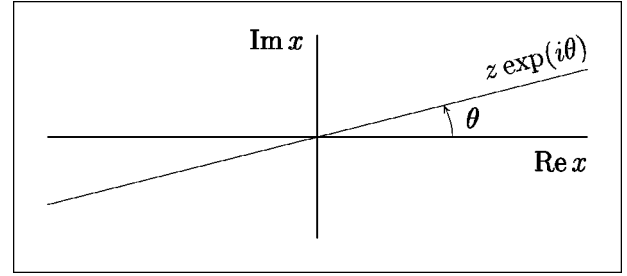


FIG. 2. Rotated path for integration of the differential equations for the functions  $F_{nl}^{(\pm)}(E, x)$  in the case of long-range potentials.

for any rotational angle  $\theta$  in the interval  $0 \leq |\theta| \leq \theta_{\max} < \pi/2$ . Then, first, according to the existence theorem (see, for example, Ref. 16), the solutions  $\phi_n(E, x)$  of Eq. (3) are holomorphic functions of  $x$  within the corresponding domain of the  $x$  plane and, secondly, they have the asymptotic behavior of the type (10) along any line (33). Moreover, the coefficients  $a(E)$ ,  $b(E)$ ,  $a'(E)$ , and  $b'(E)$  in such asymptotics are the same for all choices of the rotation angle because they do not depend on  $x$ .

Therefore, the limiting values  $F_{nl}^{(\pm)}(E, \pm\infty)$  can be found as the corresponding coefficients in the asymptotics

$$\begin{aligned} \phi_n(E, z e^{i\theta}) \rightarrow \begin{cases} F_{nL}^{(+)}(E, -\infty) e^{ik_L x} + F_{nL}^{(-)}(E, -\infty) e^{-ik_L x}, & z \rightarrow -\infty, \\ F_{nR}^{(+)}(E, +\infty) e^{ik_R x} + F_{nR}^{(-)}(E, +\infty) e^{-ik_R x}, & z \rightarrow +\infty, \end{cases} \end{aligned} \quad (34)$$

where  $x$  is given by Eq. (33) and, according to the conditions (28) and (27), when calculating  $F_{nl}^{(+)}(E, \pm\infty)$ , we have to use such  $\theta$  that  $\text{Im } k_l x \leq 0$  while in order to find  $F_{nl}^{(-)}(E, \pm\infty)$  we have to make the rotation in the opposite direction securing that  $\text{Im } k_l x \geq 0$ . Practically the coefficients of Eq. (34) can be found by solving Eqs. (13) in which the independent variable  $x$  is replaced by  $z$ , i.e.,

$$\begin{aligned} \partial_z F_{nl}^{(+)}(E, z e^{i\theta}) &= \frac{\exp(i\theta - ik_l z e^{i\theta})}{2ik_l} [V(z e^{i\theta}) - V_l] \\ &\quad \times [e^{ik_l x} F_{nl}^{(+)}(E, x) + e^{-ik_l x} F_{nl}^{(-)}(E, x)], \\ \partial_z F_{nl}^{(-)}(E, z e^{i\theta}) &= -\frac{\exp(i\theta + ik_l z e^{i\theta})}{2ik_l} [V(z e^{i\theta}) - V_l] \\ &\quad \times [e^{ik_l x} F_{nl}^{(+)}(E, x) + e^{-ik_l x} F_{nl}^{(-)}(E, x)]. \end{aligned} \quad (35)$$

If  $V(x)$  is an analytic function on the whole  $x$  plane, then starting from the boundary values (14) and (15) at  $z=0$ , these equations should be solved in both directions  $z \rightarrow \pm\infty$ , until the solutions attain their limiting values at sufficiently large  $|z|$ . When the potential is discontinuous (sequence of square wells, for example) near  $x=0$  and has analytic tails in the outer regions, we can integrate Eqs. (13) from  $x=0$  to the point where the tail begins, and from that point turn into the complex  $x$  plane.

If we choose the rotation angle  $\theta$  such that  $\text{Im } k_l x \leq 0$ , then at large distances only  $F_{nl}^{(+)}$  converges to a constant value while  $F_{nl}^{(-)}$  diverges. This, however, does not affect the first of Eqs. (35) since the second term of Eq. (11) becomes negligible as compared with the first. In other words, at large distances the first equation of the system (35) decouples from the second. If the rotation makes  $\text{Im } k_l x \geq 0$ , then  $F_{nl}^{(+)}$  diverges but the second equation of Eq. (35), decoupled from the first, gives a finite  $F_{nl}^{(-)}$  when  $|z| \rightarrow \infty$ .

In the general case, to obtain a full solution of the problem, i.e., the  $S$  matrix (25), for a complex  $E$ , we have to solve Eqs. (35) twice: First, to calculate  $||f^{(-)}(E)||$  using an appropriate (positive) rotation angle and secondly to calculate  $||f^{(+)}(E)||$  using the rotation in the opposite direction. Practically, however, very seldom do we need to solve these equations twice. Indeed, to locate the bound and resonant states, by solving Eq. (18), it is enough to calculate the matrix  $||f^{(-)}(E)||$  as the limit (19) which exists when  $\text{Im } k_l x \geq 0$ , i.e., with positive rotation angle. For the scattering states, on the real axis, all necessary limits always exist simultaneously. The only case when we may need the elements of the matrix  $||f^{(+)}(E)||$  at complex  $E$  is for the determination of the partial widths (see Appendix B).

Therefore, performing complex rotation of the coordinate, i.e., replacing Eq. (13) with (35), we are able to obtain complete solution of the one-dimensional quantum mechanical problem at any complex energy and with any potential obeying the condition (2). The rotation is only needed, however, when the potential has long-range tails.

## VI. NUMERICAL EXAMPLES

### A. Nonsymmetric square well

Demonstrating the accuracy and effectiveness of the proposed method, we start with a simple example which does not require the complex rotation. This is the asymmetric square well shown in Fig. 3 and defined as

$$V(x) = \begin{cases} V_1, & x \leq -a, \\ V_2, & -a < x < +a, \\ V_3, & x \geq +a, \end{cases} \quad (36)$$

TABLE I. Lower part of the spectrum of bound and resonant states calculated, using the Jost matrix method, for the asymmetric square-well potential (36). The energies and widths are given in arbitrary units such that  $\hbar^2/2m = 1$ .

Re $E$	$\Gamma$	$\Gamma_L$	$\Gamma_R$
-8.4837914199	0	0	0
-4.1436976719	0	0	0
1.7058170112	2.4975286589	2.4975286589	0
25.5180711001	26.1093154827	21.1232875500	4.9860279327
46.7168461195	41.4802081079	31.3236139533	10.1565941546
72.9499239777	57.7898887368	42.1161727017	15.6737160351
104.2041854350	75.0092249117	53.5123817895	21.4968431222
140.4640465022	93.0507392863	65.4578827056	27.5928565807
181.7173066134	111.8304535757	77.8978089153	33.9326446604

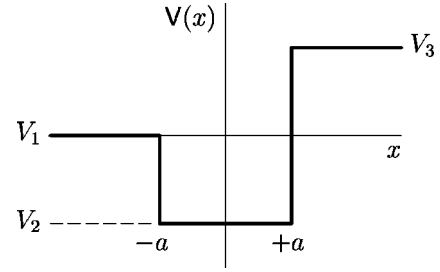


FIG. 3. Asymmetric potential well of width  $2a$ . The parameters used in the calculations are  $V_L = V_1 = 0$ ,  $V_2 = -10$ ,  $V_R = V_3 = 10$ ,  $a = 1$  (in the arbitrary units for which  $\hbar^2/2m = 1$ ).

where  $a = 1$ ,  $V_1 = 0$ ,  $V_2 = -10$ , and  $V_3 = 10$  in the arbitrary units such that  $\hbar^2/2m = 1$ . This problem can be easily solved analytically by the smooth matching of the plane waves at  $x = \pm a$ . A solution that has only outgoing waves outside the interval  $[-a, +a]$  exists if and only if

$$k_2(k_1 + k_3)\cos(2k_2a) - i(k_1k_3 + k_2^2)\sin(2k_2a) = 0, \quad (37)$$

where  $k_j = \sqrt{(E - V_j)2m/\hbar^2}$ . Such a solution describes a bound state when  $E$  is negative (on the physical sheet of the Riemann surface; see Appendix A), and a resonance when  $E$  is above  $V_1$  and has a negative imaginary part (on the unphysical sheet). Therefore, the roots of Eq. (37) give us exact values of the binding and resonant energies with which the corresponding spectrum generated by the Jost matrix method can be compared.

When obtaining this spectrum from Eqs. (13), we do not make use of the simplicity of  $V(x)$ . These equations are solved numerically in the both directions starting from  $x = 0$  with the boundary conditions (14), (15). The integration is terminated at the points  $x = \pm a$  beyond which the right-hand sides of Eqs. (13) vanish and the Jost solutions  $F_{nl}^{(\pm)}(E, x)$  do not change, having attained their final values  $F_{nL}^{(\pm)}(E, -\infty)$  and  $F_{nR}^{(\pm)}(E, +\infty)$  that are used to construct the Jost matrices  $||f^{(\pm)}(E)||$  according to Eqs. (19) and (24). Changing  $E$  and repeating the calculations, we can locate (using, for example, the Newton method) the points on the complex  $E$  plane where  $\det||f^{(-)}(E)|| = 0$ , i.e., the spectral points of the given potential.

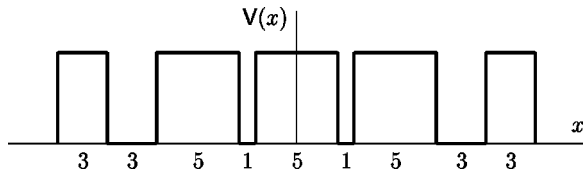


FIG. 4. Symmetric quadruple-well heterostructure of Ref. 7. The heights of all barriers are equal to 230 meV. The widths of the barriers and gaps are shown underneath in nm. The resonances in this structure were located for a particle of mass  $m^* = 0.067m_e$ , where  $m_e$  is the mass of electron.

If the wave function is needed, we can keep track of  $F_{nl}^{(\pm)}(E, x)$  at the intermediate points when solving the differential equations (13). Then the physical wave function of a bound state is constructed using Eqs. (11), (16), and (17). It should be noted that the oscillating and attenuating exponential functions are included in such a wave function explicitly via the ansatz (11), and therefore  $F_{nl}^{(\pm)}(E, x)$  are rather smooth functions. Similarly, the scattering wave function together with the reflection and transmission amplitudes can be obtained if we choose  $E$  on the positive real axis.

The lower part of the spectrum thus obtained for the potential (36) is given in Table I. It includes two bound states, one resonance of the second type (that can only decay in the left channel), and the first six resonances of the first type. The Jost matrix method reproduces all the energies and widths that can be obtained from Eq. (37), with practically any desired accuracy. In Table I, the numbers are given with ten figures after the decimal point (all these figures are the same as the exact solutions), but if necessary the accuracy can be increased even further by decreasing the tolerance parameters in the numerical procedures that solve the differential equations and locate zeros of the Jost matrix determinant. It should be emphasized that the results remain accurate even if we consider very broad resonances.

In addition to the total widths of the resonances, in the third and fourth columns of Table I, the partial widths for decaying into the left and right channels are given. Within the proposed method, they can be obtained simultaneously with  $\Gamma$ , using Eq. (B6). To the best of our knowledge, no other method is able to calculate partial widths of one-dimensional resonances.

As one would expect, for the potential (36), the probability of decaying of a resonance in the left direction is significantly higher than that for the right direction. This also means that the particle approaching the potential from the left, has more chances to be trapped in one of these resonant states than the same particle moving from the right. In the case of the more complicated function  $V(x)$ , however, it is not easy to guess which direction is preferable for a resonance to decay. Knowledge of  $\Gamma_L$  and  $\Gamma_R$  gives, therefore, additional important information on the properties of the resonances.

### B. Symmetric quadruple-well heterostructure

The next example we consider is taken from Ref. 7, where the resonance spectrum of a particle with mass equal to

0.067 mass of electron, moving in the symmetric quadruple-well heterostructure shown in Fig. 4, was calculated using several different methods. The profile of the potential consists of five rectangular barriers having equal heights of 230 meV with zero potential elsewhere. The widths of the barriers are (from left to right) 3, 5, 5, 5, and 3 nm, and the gaps separating them are 3, 1, 1, and 3 nm wide. This potential is a little bit more complicated than Eq. (36), but our numerical method does not need any modifications regardless of how complicated the potential is.

Several spectral states generated by this potential are given in Table II where the results obtained by different methods are compared. As in Ref. 7, the widths of the resonances are presented in terms of their lifetimes  $\tau = \hbar/\Gamma$ . As is seen, all the digits obtained by the Argument Principle Method (APM) of Ref. 7 are correct while the other three methods [the Quantum Reflection Pole Method (QRPM), Perturbed Wavenumber Method (PWM), and Modified Density of States Method (MDOS)] are not sufficiently accurate even with this simple potential consisting of rectangular barriers.

TABLE II. The spectrum of resonant states for a particle of mass  $m^* = 0.067m_e$  (where  $m_e$  is the mass of free electron) moving in the symmetric quadruple-well potential which is shown in Fig. 4. The resonance width is given in terms of the corresponding lifetime  $\tau = \hbar/\Gamma$ .

$E$ (meV)	$\tau$ (ps)	method
129.9256515015	0.0574930342	this work
129.925	0.057	APM
130.047	0.058	QRPM
129.967	0.071	PWM
130.2957090471	0.0563038531	this work
130.296	0.056	APM
130.156	0.055	QRPM
130.310	0.067	PWM
130.376	0.070	MDOS
205.2566066390	0.3189863719	this work
205.257	0.319	APM
205.257	0.316	QRPM
205.220	0.316	PWM
205.323	0.365	MDOS
254.0528681944	0.1283002864	this work
254.053	0.128	APM
254.053	0.125	QRPM
254.061	0.136	PWM
254.094	0.135	MDOS
365.1443824466	0.0196816576	this work
365.144	0.020	APM
365.861	0.023	QRPM
365.235	0.029	PWM
365.410	0.029	MDOS
414.4454409411	0.0099325202	this work
509.7135327776	0.0065002559	this work
600.7565867563	0.0041682986	this work
698.0676599010	0.0037912730	this work

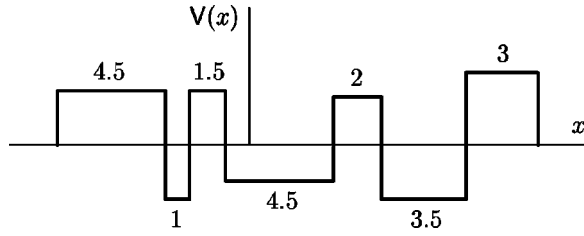


FIG. 5. Nonsymmetric quadruple-barrier heterostructure. The barrier potentials (from left to right) are 225, 225, 200, and 300 meV. Bottoms of the wells separating them, are respectively at  $-225$ ,  $-150$ , and  $-225$  meV. The widths of the barriers and gaps are shown on the figure in nm. The spectral states of this structure given in Table III, were located for a particle of mass  $m^* = 0.067m_e$ , where  $m_e$  is the mass of electron.

### C. Nonsymmetric quadruple-barrier heterostructure

Since the potential shown in Fig. 4 is symmetric, the total width  $\Gamma$  is equally divided between  $\Gamma_L$  and  $\Gamma_R$ . This is why the partial widths are not given in Table II. In the next example (see Fig. 5) there is no symmetry or any clear way to say which direction is preferable for resonances to decay. And indeed, as one can see in Table III, some of them tend to decay into the left while the others into the right channel. This tendency cannot be guessed from studying the energy dependence of the reflection and transmission coefficients. In general, the information on analytic structure of the  $S$  matrix, i.e., knowledge of the distribution of its poles in the complex energy plane, gives much more than detailed scattering characteristics. Thus, the transmission coefficient shown in Fig. 6, has only three clear peaks that correspond to narrow resonances while the broad resonances are not seen against the background and each other. An extreme case of such resonance “hiding” is demonstrated by the next example, where the transmission coefficient does not show any irregularities whatsoever.

### D. Potential with infinite tails

All three potentials we considered so far are of finite range, i.e., they become constant at finite distances from  $x = 0$ . This means that we need to integrate Eqs. (13) only on a finite interval  $x_1 \leq x \leq x_2$  outside of which the right-hand

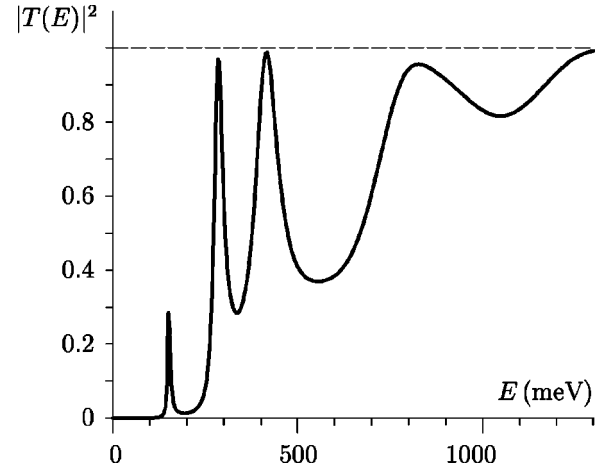


FIG. 6. Energy dependence of the transmission coefficient for the nonsymmetric quadruple-well heterostructure shown in Fig. 5.

sides of these equations vanish and the functions  $F_{nl}^{(\pm)}(E, x)$  do not change. Let us consider now a case when the potential has tails extending to infinity. An example of such a potential is shown in Fig. 7 and defined as

$$V(x) = \begin{cases} V_1 x^2 \exp(+\mu_1 x), & x < 0, \\ V_2 x^2 \exp(-\mu_2 x), & x \geq 0, \end{cases} \quad (38)$$

where  $V_1 = 10$ ,  $V_2 = 20$ ,  $\mu_1 = 1$ , and  $\mu_2 = 2$  in the arbitrary units such that  $\hbar^2/2m = 1$ .

It might seem that the tails are insignificant because they vanish very rapidly when  $|x|$  increases. This is true when the scattering is concerned (calculation of the transmission coefficient at real positive energies). Although even in this case, in order to achieve high accuracy, one has to take into account the interaction at rather long distances. However, when it comes to resonances, the presence of the tails has some nontrivial consequences and cannot be ignored.

It is shown in Appendix A that the limit (19) defining the Jost matrix, exists only if the point  $E$  is on or above the unitary cuts (see Fig. 1) which are along the real positive axis when the rotation angle  $\theta = 0$ . This also means that for any point below the cuts the elements of the matrix on the right-hand side of Eq. (19) diverge when  $|x|$  increases. This

TABLE III. Lower part of the spectrum of bound and resonant states calculated, using the Jost matrix method, for the nonsymmetric quadruple-barrier heterostructure shown in Fig. 5.

Re $E$ (meV)	$\Gamma$ (meV)	$\Gamma_L$ (meV)	$\Gamma_R$ (meV)
-73.8492200705	0	0	0
-31.3309516367	0	0	0
151.3121881936	6.9709902700	6.3462911249	0.6246991451
282.9329059403	27.8291339527	16.7703085398	11.0588254128
410.6371295776	75.9212736352	44.5409201457	31.3803534895
541.7594328710	258.7348042047	254.5090164605	4.2257877443
759.4317036555	247.1716665063	117.6181561005	129.5535104058
917.1817136188	378.1741780097	146.8361399247	231.3380380849
1189.8521293731	478.8772625385	430.4969782256	48.3802843129

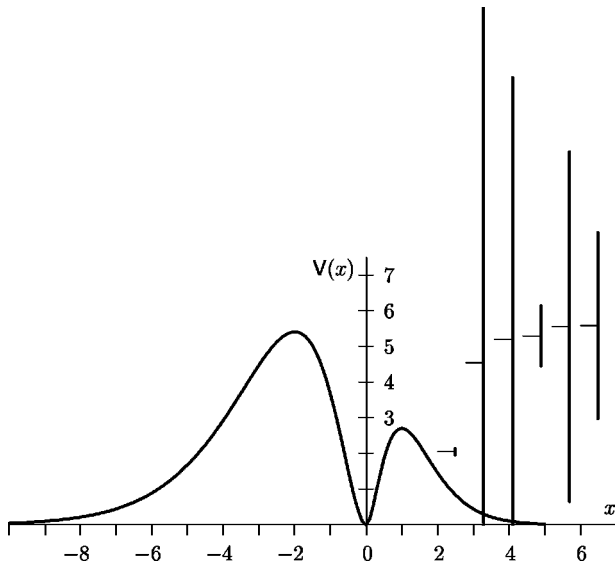


FIG. 7. Two-barrier potential, defined by Eq. (38), with the tails extending to infinity in both directions. The energy and distance are measured in arbitrary units such that  $\hbar^2/2m=1$ . The resonance energies are shown by horizontal lines and their widths by vertical bars. These spectral points are also given in Table IV and shown in Fig. 10.

divergency is caused by the tails of the potential despite their fast (exponential in this example) vanishing.

Figures 8 and 9 illustrate these statements as well as the fact that the limit (19), i.e., values of the elements of the Jost matrix, does not depend on the choice of  $\theta$  if this angle is such that the point  $E$  is above the cuts. To avoid complicated

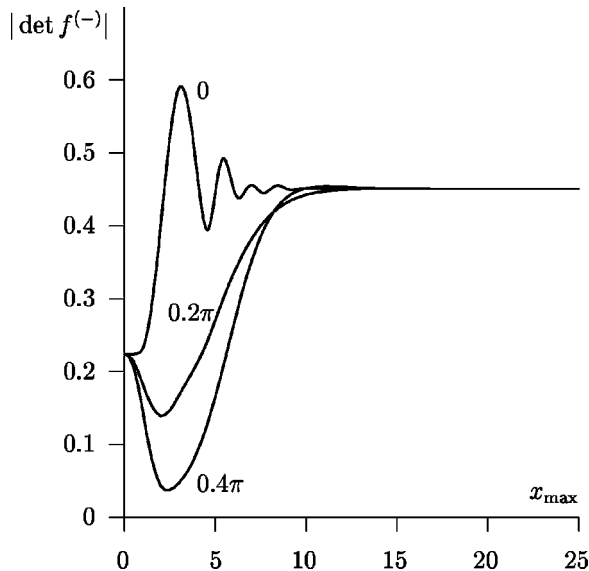


FIG. 8. Absolute value of the Jost matrix determinant for the two-barrier potential (38), as a function of maximal distance  $x_{\max}$  to which the differential equations (35) are integrated and which, therefore, stands for the infinity in Eq. (19). All the curves correspond to the same real energy  $E=5$  but to different choices of the rotation angle  $\theta$  shown next to them. The energy and distance are in arbitrary units such that  $\hbar^2/2m=1$ .

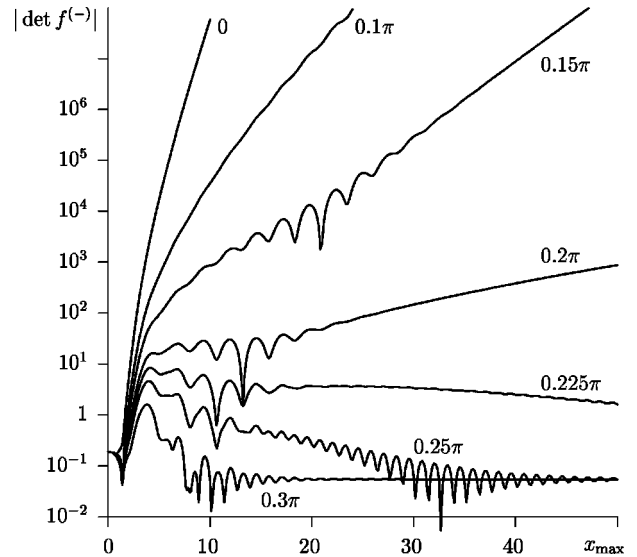


FIG. 9. Absolute value of the Jost matrix determinant for the two-barrier potential (38), as a function of maximal distance  $x_{\max}$  to which the differential equations (35) are integrated and which, therefore, stands for the infinity in Eq. (19). All the curves correspond to the same complex energy  $E=5-i5$  but to different choices of the rotation angle  $\theta$  shown next to them. The energy and distance are in arbitrary units such that  $\hbar^2/2m=1$ .

monitoring of individual matrix elements, the value of  $|\det f^{(-)}(E)|$  was calculated as a function of the real parameter  $x_{\max}$  which effectively served as “infinity” in Eq. (19). More precisely, Eqs. (35) were solved from  $z=0$  to  $z=-x_{\max}$  in the left direction and to  $z=x_{\max}/2$  in the right direction (because the right tail decays faster). In other words, the left and right tails of the potential were cut at  $z=-x_{\max}$  and  $z=x_{\max}/2$ , respectively. The determinant was then calculated by substituting into Eq. (19) the values of  $F_{nL}^{(+)}(E, -x_{\max}e^{i\theta})$  and  $F_{nR}^{(-)}(E, x_{\max}e^{i\theta}/2)$  thus obtained.

Since  $V_L=V_R=0$ , the left and right channel thresholds for the potential (38) as well as the corresponding unitary cuts coincide. Both cuts start from  $E=0$  and run to infinity along the real axis. When  $\theta>0$  they turn down together and thus expose the points of the  $E$  plane above them. For the point  $E=5$  on the real axis, Fig. 8 shows how the right-hand side of Eq. (19) converges to its limit with three choices of the rotation angle, namely,  $0$ ,  $0.2\pi$ , and  $0.4\pi$ . The convergence becomes faster when this angle increases.

Apparently, for different  $\theta$ , Eqs. (35) and therefore their solutions, i.e., functions  $F_{nl}^{(\pm)}(E, x)$ , are quite different. However, despite different behaviors at small  $|x|$ , they eventually converge to the same limits  $F_{nl}^{(\pm)}(E, \pm\infty)$  if  $E$  is above the cuts. This remarkable fact suggests a very simple and reliable way of controlling the accuracy of the calculations. Indeed, we can repeat the calculation for a particular value of  $E$  using two or three different values of  $\theta$ . Then the digits (in the value of transmission coefficient or resonance energy, for example) that remain the same, i.e., are  $\theta$  independent, can be considered as exact because the probability of coincidence is negligible.

In the case under consideration, such an analysis shows

TABLE IV. Spectral points calculated, using the Jost matrix method, for the two-barrier potential defined by Eq. (38) and shown in Fig. 7. Energies are given in arbitrary units such that  $\hbar^2/2m = 1$ . These spectral points are shown in Fig. 10.

$\text{Re } E$	$\Gamma$	$\Gamma_L$	$\Gamma_R$
2.0480027780	0.1909349562	0.0000120286	0.1909229276
4.5428598416	19.9110037394	2.6595868957	17.2514168437
5.1944714957	14.6973943851	1.9210051579	12.7763892273
5.2940624464	1.7007155642	0.3838049449	1.3169106193
5.5532015404	9.8209883494	1.2869433510	8.5340449984
5.5849886470	5.2292359995	0.8604715925	4.3687644070

that the accuracy of ten digits in the value of  $|\det f^{(-)}(5)| = 0.4510841955$  is achieved when  $x_{\max} \geq 30$  with  $\theta = 0$ . For the points in the fourth quadrant of the  $E$  plane, the convergence is slower and also improves with increasing  $\theta$ . For the point  $E = 5 - i5$ , this is illustrated in Fig. 9. When  $\theta$  is small, the Jost matrix at this energy does not converge at all in accordance with formal considerations given in Appendix A. With  $\theta = 0.3\pi$ , the last digit in  $|\det f^{(-)}(5 - i5)| = 0.0548640248$  stabilizes after the  $x_{\max}$  reaches 60. When  $\theta = 0.25\pi$ , the same result is obtained with  $x_{\max} \geq 90$ . When  $\theta = 0.225\pi$ , only the first three digits (0.0549) are stable even at  $x_{\max} = 150$ .

The resonances of the potential (38) found using appropriate values of  $\theta$  (that move the unitary cuts below the corresponding spectral points), are given in Table IV and shown in Figs. 7 and 10. The remarkable feature of this resonance spectrum is the fact that all the resonances overlap and, except for the first one, are very broad. Because of this, the potential (38) would be a real challenge for any method designed for locating resonances. Apparently, only the complex-energy methods would be able to locate them. Indeed, at real energies the transmission coefficient (see Fig. 11) does not show any peaks or even small bumps. Such a potential could therefore serve as a testing ground (a tough one) for new methods.

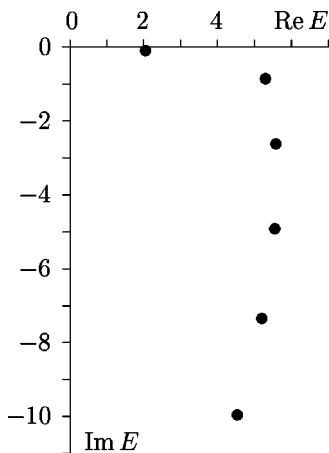


FIG. 10. Spectral points of Table IV for the two-barrier potential, defined by Eq. (38) and shown in Fig. 7. The energy is in arbitrary units such that  $\hbar^2/2m = 1$ .

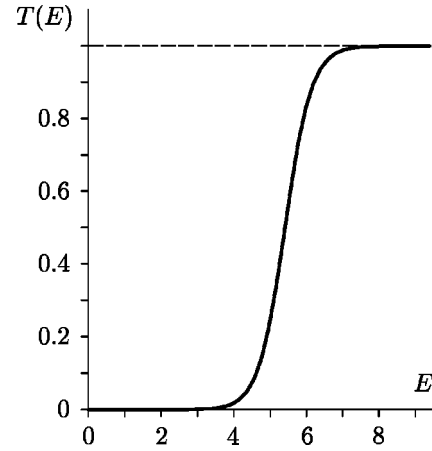


FIG. 11. Energy dependence of the transmission coefficient for the two-barrier potential, defined by Eq. (38) and shown in Fig. 7. The energy is in arbitrary units such that  $\hbar^2/2m = 1$ .

## VII. CONCLUSION

A combination of the variable-constant method with the complex coordinate rotation is used to replace one-dimensional Schrödinger equation by an equivalent system of linear first-order differential equations whose solutions, taken at long distances from the interaction region, form the Jost matrix. Zeros of its determinant in the complex-energy plane correspond to the spectral points that include bound states and resonances. In addition to determining total widths of resonances, a simple but exact procedure is proposed for calculating their partial widths that show relative probabilities of resonance decaying into the left and right channels.

The proposed equations not only solve the problem of locating spectral points for an arbitrary potential profile, but give a complete solution of the one-dimensional Schrödinger equation at any complex energy, i.e., they also give the corresponding wave functions as well as the transmission and reflection amplitudes.

The effectiveness and accuracy of the method are demonstrated by several numerical examples. A reliable way of accuracy control based on calculations with different rotation angles, is used. It is shown that the proposed method is able to locate even extremely wide and overlapping resonances as well as adequately take into account long-range tails of the potential.

In the real-life problems concerning one-dimensional semiconductor nanostructures, there is an additional complication caused by the fact that the effective mass of the charge carriers (electrons or holes) is different inside semiconductor layers with different chemical compositions. This problem was not discussed in the present paper simply because of the size limitations. Actually, these mass variations can be nicely fitted in the suggested Jost matrix theory. This is done by constructing the Jost matrix in a way similar to the well-known transfer-matrix method. However, in contrast to the traditional transfer-matrix method, where the potential profile must be discretized by a sequence of thin elements of rectangular shape with constant potential energy, within the Jost matrix approach the transfer matrix is calculated directly for an arbitrary potential. This is achieved by using two lin-

early independent solutions (11) of Eqs. (13) instead of the plane waves, on each segment of the line where the effective mass is constant. This generalized transfer-matrix method will be published in a forthcoming article together with the extension of the Jost matrix theory, suitable for potentials having Coulomb tails and nanostructures placed in a strong electric field.

### ACKNOWLEDGMENT

Financial support from National Research Foundation of South Africa, University of South Africa, and the Joint Institute for Nuclear Research (Dubna) is greatly appreciated.

### APPENDIX A: ASYMPTOTICS OF $F^{(\pm)}$

To analyze the behavior of the functions  $F_{nl}^{(\pm)}(E, x)$  at large  $|x|$  we rewrite the system (13) in the following compact form:

$$\partial_x F_{nl}^{(\pm)}(E, x) = \pm \frac{e^{\mp ik_l x}}{2ik_l} [V(x) - V_l] \phi_n(E, x), \quad l=L, R, \quad (\text{A1})$$

where  $\phi_n(E, x)$  is given by Eq. (11). It is clear that if the limits  $\lim_{x \rightarrow \pm \infty} F_{nl}^{(\pm)}(E, x)$  exist then the derivatives at the left-hand side of Eqs. (A1) vanish when  $x \rightarrow \pm \infty$ , which implies vanishing of the products  $\exp(\mp ik_l x)[V(x) - V_l]\phi_n$ . The converse statement, i.e., the existence of these limits as a result of vanishing of the right-hand sides of Eqs. (A1), is not generally true. For our purpose, however, it is enough to know that if the right-hand sides of Eqs. (A1) vanish faster than  $1/|x|$ , then the limits  $\lim_{x \rightarrow \pm \infty} F_{nl}^{(\pm)}(E, x)$  do exist. Indeed, for any function  $\varphi(r)$ , the behavior of its derivative

$$\frac{d\varphi(r)}{dr} \underset{r \rightarrow \infty}{\sim} r^{-(\epsilon+1)}, \quad \epsilon > 0,$$

is a sufficient condition for existence of its limit at large  $r$  since the asymptotic behavior of  $\varphi(r)$  can be written as

$$\varphi(r) \underset{r \rightarrow \infty}{\sim} \int r^{-(\epsilon+1)} dr = \left( \text{const} - \frac{1}{\epsilon r^\epsilon} \right) \underset{r \rightarrow \infty}{\rightarrow} \text{const}.$$

Therefore, at those values of (complex)  $E$  at which the products  $\exp(\mp ik_l x)[V(x) - V_l]\phi_n$  vanish faster than  $1/|x|$  when  $x \rightarrow \pm \infty$ , the functions  $F_{nl}^{(\pm)}(E, x)$  have finite limits determining the Jost matrices (19) and (24).

In many practical applications the potential becomes identically constant  $V(x) \equiv V_l$  at large  $|x|$  and hence the Jost matrices exist for all complex  $E$ 's. However, in the general case defined by Eq. (2), the long-range behavior of the right-hand sides of Eqs. (A1) depends on the choice of the point  $E$  in the complex energy plane. Indeed, the choice of  $E$  determines the behavior of the exponential functions  $\exp(\mp ik_l x)$  as well as the basic solutions  $\phi_n(E, x)$  that can be oscillating, growing, or vanishing.

Since the functions  $F_{nl}^{(\pm)}(E, x)$ , and therefore the Jost matrices (19) and (24), depend on the energy  $E$  via the channel momenta  $k_L = \sqrt{(2m/\hbar^2)(E - V_L)}$  and  $k_R = \sqrt{(2m/\hbar^2)(E - V_R)}$ , there are two square-root branching

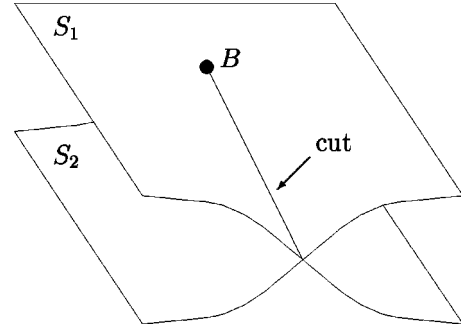


FIG. 12. Fragments of the physical ( $S_1$ ) and unphysical ( $S_2$ ) sheets of the complex-energy Riemann surface around a branching point ( $B$ ) that corresponds to a threshold energy ( $V_L$  or  $V_R$ ). Transition from  $S_1$  to  $S_2$  and back is possible through the unitary cut running from  $B$  to infinity.

points for these matrices in the energy plane, namely,  $E = V_L$  and  $E = V_R$ . This means that if we make two full circles around either of these points then matrix elements of  $||f^{(\pm)}(E)||$  return to the same values from which the circling was started (one full circle is not enough). This is because the channel momentum

$$k_l = \sqrt{(2m/\hbar^2)|E_l|} e^{i\chi_l} = \sqrt{(2m/\hbar^2)|E_l|} e^{i\chi_l/2} \quad (\text{A2})$$

comes to its initial value when  $\chi_l \rightarrow \chi_l + 4\pi$ , where  $|E_l|$  and  $\chi_l$  are the polar coordinates of the point  $E$  on the energy-plane relative to the branching point  $V_l$ , i.e.,

$$E = V_l + |E_l| e^{i\chi_l}. \quad (\text{A3})$$

In other words, elements of the Jost matrix have two different values at each point  $E$  on this circle.

In order to make the Jost matrix a single-valued function of  $E$ , we can assume (as is usual in the complex analysis) that the complex energy forms the so-called Riemann surface consisting of several parallel sheets. When doing the first circle around a branching point, we are moving on the first sheet and then continue on the second one until coming back to the first sheet after completing the two full circles. Such a continuous transition from one sheet to another is possible if we make a cut from the branching point to infinity, and connect opposite rims of the cuts on the two sheets (see Fig. 12).

As is usual in scattering theory, we make straight line cuts from both branching points to infinity along the positive real axis. Each of the two sheets related by the first branching point, is further branched at the second branching point. Therefore the full Riemann surface consists of four parallel sheets. We can reach any of these sheets by making an appropriate number of circles around the first and second branching points.

The physical energy (at which scattering takes place) is on the positive real axis. We choose the cuts and their interconnections in such a way that the physical scattering energies lie on the upper rims of both cuts. Starting from these physical energies and moving in an anticlockwise direction around all branching points, we cover the so-called physical sheet of the energy plane. According to Eq. (A2) the channel momenta corresponding to this sheet have positive imaginary

parts. The bound states are also on the physical sheet (this is necessary to guarantee the exponential attenuation of their wave functions). The resonances, however, correspond to zeros of the Jost-matrix determinant at the momenta with negative imaginary parts [see Eq. (6) showing the resonant boundary conditions] and therefore lie on the unphysical sheet of the Riemann surface. The resonances that are able to decay in both directions (both channels) must have  $\text{Im}(k_L) < 0$  and  $\text{Im}(k_R) < 0$ . This means that they lie on the sheet which is unphysical with respect to both branching points.

In practical calculations, we can choose points on one of the four Riemann sheets by selecting appropriate signs in front of the square roots (5) for  $k_L$  and  $k_R$ , i.e., appropriate signs of their imaginary parts. We assume that  $V(x)$  is an analytic function of  $x$  and satisfies the condition

$$\lim_{|x| \rightarrow \infty} x[V(x) - V_l] = 0 \quad (\text{A4})$$

within the sectors swept by the line  $x = z \exp(i\theta)$  shown in Fig. 2, when

$$-\theta_{\max} \leq \theta \leq \theta_{\max}, \quad 0 < \theta_{\max} < \pi/2$$

with a large enough  $\theta_{\max}$ . It is obvious that if the Jost matrices exist for certain potential, then they also exist for all other potentials that have faster decaying tails. Therefore, if we find the domains of their existence in the  $E$  plane for the “worst case,” namely,

$$V(x) \Big|_{|x| \rightarrow \infty} \left( \frac{\text{const}}{x^{1+\varepsilon}} + V_l \right), \quad \varepsilon > 0, \quad l = L, R, \quad (\text{A5})$$

then for all other potentials obeying the condition (A4), the Jost matrices exist at least in the same domains.

Under the condition (A5), the behavior of the general solution of Eq. (3) at large distances is of the exponential character. A rigorous proof of this can be found, for example, in Ref. 22. For our purpose it is enough to simply apply the WKB approximation that gives the leading terms of the asymptotics behavior of the two linearly independent solutions of Eq. (3) at large  $|x|$  in the form

$$\begin{aligned} \Psi_{1,2}(E, x) &\Big|_{|x| \rightarrow \infty} \frac{1}{\sqrt[4]{4k^2 - V(x)}} \exp \left[ \pm i \int^x \sqrt{k^2 - V(x')} dx' \right] \\ &= \frac{1}{\sqrt[4]{k^2 - V(x)}} \\ &\quad \times \exp \left[ \pm i \int^x \sqrt{k^2 - V_l - \frac{\text{const}}{x'^{1+\varepsilon}}} dx' \right] \\ &\approx \frac{1}{\sqrt[4]{k^2 - V(x)}} \exp \left[ \pm i \int^x \left( k_l - \frac{\text{const}}{2x'^{1+\varepsilon}} \right) dx' \right]. \end{aligned}$$

Since  $\varepsilon > 0$ , the integration of  $x^{-1-\varepsilon}$  gives a vanishing term

$$\Psi_{1,2}(E, x) \propto \frac{1}{\sqrt{k_l}} \exp \left[ \pm i \left( k_l x + \frac{\text{const}}{2\varepsilon x^\varepsilon} \right) \right],$$

and at large  $|x|$  we remain with the exponential function  $\propto \exp(\pm ik_l x)$ . Therefore the basic solutions  $\phi_n(E, x)$  of Eq. (3) defined by Eqs. (8) and (9), have the form

$$\begin{aligned} \alpha_n e^{+ik_L x} + \alpha'_n e^{-ik_L x} \xrightarrow[-\infty \leftarrow x]{x \rightarrow +\infty} \phi_n(E, x) \xrightarrow{x \rightarrow +\infty} \beta'_n e^{+ik_R x} \\ + \beta_n e^{-ik_R x}, \end{aligned} \quad (\text{A6})$$

where  $\alpha_n$ ,  $\alpha'_n$ ,  $\beta'_n$ , and  $\beta_n$  are  $x$ -independent coefficients.

When  $\text{Im}(k_l x) = 0$  all terms of this asymptotics are oscillating and hence the solutions  $\phi_n(E, x)$  are bounded, i.e., there are such constants  $\Phi_n$  that

$$|\phi_n(E, x)| \leq \Phi_n \quad \text{when } |x| \rightarrow \infty.$$

The exponential functions in Eq. (A1) are also bounded  $|\exp(\mp ik_l x)| = 1$  when  $\text{Im} k_l x = 0$ . Together with the condition (A4) this means that the right-hand sides of Eqs. (A1) vanish at large  $|x|$  faster than  $1/|x|$  and therefore the Jost matrices exist.

When  $\text{Im}(k_l x) > 0$  the situation is more complicated because the asymptotics (A6) of the basic solutions involve both the growing and vanishing terms. To simplify further derivations, we can rewrite Eq. (A6) in the following compact form:

$$\phi_n(E, x) \Big|_{|x| \rightarrow \infty} \zeta_{nl} e^{+ik_l x} + \xi_{nl} e^{-ik_l x}, \quad (\text{A7})$$

where, as usual, the subscript  $l$  should be replaced by  $L$  or  $R$  when we consider the far left or right end of the  $x$  axis, respectively, while  $\zeta_{nl}$  and  $\xi_{nl}$  are the corresponding coefficients in the asymptotics (A6), namely,  $\zeta_{nL} = \alpha_n$ ,  $\zeta_{nR} = \beta'_n$ ,  $\xi_{nL} = \alpha'_n$ , and  $\xi_{nR} = \beta_n$ . Combining this with Eq. (A1), we see that

$$\begin{aligned} \partial_x F_{nl}^{(\pm)}(E, x) &\Big|_{|x| \rightarrow \infty} \frac{e^{\mp ik_l x}}{2ik_l} [V(x) - V_l] (\zeta_{nl} e^{+ik_l x} + \xi_{nl} e^{-ik_l x}) \\ &= \begin{cases} + \frac{1}{2ik_l} [V(x) - V_l] (\zeta_{nl} + \xi_{nl} e^{-2ik_l x}) & \text{for } (+), \\ - \frac{1}{2ik_l} [V(x) - V_l] (\zeta_{nl} e^{+2ik_l x} + \xi_{nl}) & \text{for } (-). \end{cases} \end{aligned} \quad (\text{A8})$$

Since  $\exp(-2ik_l x)$  is growing while  $\exp(+2ik_l x)$  is vanishing when  $\text{Im} k_l x > 0$ , the function  $F_{nl}^{(-)}(E, x)$  does have a finite limit in this case and  $F_{nl}^{(+)}(E, x)$  does not.

When  $\text{Im}(k_l x) < 0$  as can be seen from the same Eq. (A8), we have just the opposite case, namely, the limit of  $F_{nl}^{(+)}(E, x)$  does exist while that of  $F_{nl}^{(-)}(E, x)$  does not.

Looking at the Jost matrices (19) and (24), we see that all the elements of  $\|f^{(-)}(E)\|$  and  $\|f^{(+)}(E)\|$  exist when  $\text{Im} k_l x \geq 0$  and  $\text{Im} k_l x \leq 0$ , respectively. These two matrices exist simultaneously only on the dividing lines  $\text{Im} k_l x = 0$ , ( $l = L, R$ ). Using Eqs. (13), we can therefore calculate the matrix  $\|f^{(-)}(E)\|$  on and above these lines and the matrix  $\|f^{(+)}(E)\|$  on and below them. For real  $x$ , these lines

coincide with the cuts (along the positive real axis) that separate the physical and unphysical domains of the complex  $E$  surface.

It should be emphasized that, as follows from the general theory of multichannel scattering (see, for example, Ref. 18), for physically reasonable potentials (without peculiar behavior such as nonintegrable singularities, for instance) the Jost matrix and its conjugate partner exist and are analytic functions of  $E$  in all areas of the complex  $E$  plane that are physically interesting (where the bound, scattering, and resonant states are situated). Therefore, when we say that the Jost matrix does not exist at certain values of  $E$ , this simply means that, without modification (complex rotation), our Eq. (13) produce diverging results for the limits (19) or (24).

By considering complex  $x$ , we can do the analytic continuation of  $\|f^{(\pm)}(E)\|$  across the dividing lines to the domains where Eqs. (13) do not give finite values for these matrices. For example, the dividing lines can be turned downwards to expose the resonance spectral points, by rotating  $x$  as given by Eq. (33). Indeed, if  $\chi_l$  is the polar angle parameterizing the position of a point on the  $E$  plane relative to the branching point  $V_l$ , then by choosing large enough  $\theta$  we can make  $\text{Im } k_l x$ ,

$$\text{Im } k_l x = \text{Im}(|k_l|z e^{i(\theta + \chi_l/2)}) = |k_l|z \sin(\theta + \chi_l/2), \quad (\text{A9})$$

positive even when  $\chi_l$  is negative (when the point  $E$  is below the cut, i.e., on the unphysical sheet) and vice versa. From the last equation is clear that when  $\theta > 0$  both dividing lines are turned down by  $2\theta$  (see Fig. 1).

It is worthwhile to mention that the ultimate separation of the domains of the complex  $E$  plane by the dividing lines takes place only in the ‘‘worst case’’ when the potential has slowly decaying tails. If, however, the potential decays at large  $|x|$  exponentially, then the matrix  $\|f^{(+)}(E)\|$  also exists within a band above the dividing lines and the matrix  $\|f^{(-)}(E)\|$  in the symmetric bands below them. The faster the potential decays the wider this band is.

For example, if the potential decays as  $\sim \exp(-\mu x)$  at the right end of the  $x$  axis, then according to Eq. (A8), the derivative  $\partial_x F_{nR}^{(-)}(E, x)$  below the dividing line ( $\text{Im } k_R x < 0$ ) behaves as

$$\begin{aligned} \partial_x F_{nR}^{(-)}(E, x) &\sim e^{-\mu x} e^{2ik_R x} \\ &= e^{i(2 \text{Re } k_R x - \mu \text{Im } x)} \exp(-2 \text{Im } k_R x - \mu \text{Re } x). \end{aligned}$$

The last exponential function decays at large distances if  $\text{Im } k_R x > -(\mu/2) \text{Re } x$ , i.e., when

$$|k_R| \sin(\theta + \chi/2) > -\frac{\mu}{2} \cos \theta. \quad (\text{A10})$$

If  $\theta = 0$ , this condition reads  $\text{Im } k_R > -\mu/2$  which means that  $F_{nR}^{(-)}(E, +\infty)$  exists not only for all points of the physical sheet but also on the unphysical sheet in the immediate vicinity of the cut.

## APPENDIX B: PARTIAL WIDTHS

As was mentioned in Sec. II, the total width  $\Gamma$  is a sum of the partial widths  $\Gamma_L$  and  $\Gamma_R$  that determine the decay probabilities for the left and right channels (directions). A simple way to show this and to develop a procedure for calculating  $\Gamma_L$  and  $\Gamma_R$ , is to consider the  $S$  matrix near the point  $E_r = E_{\text{res}} - i\Gamma/2$ .

First of all, we notice that when the collision energy becomes very high (goes to infinity) the incoming waves are transmitted through the potential almost completely, i.e., the transmission amplitudes  $T_l$  in Eq. (26) tend to some complex numbers  $e^{i\delta_l}$  that give 1 for the transmission coefficients  $|T_l|^2$ , while the reflection amplitudes tend to zero. Keeping this in mind, we write the matrix function  $S(E)$  as follows:

$$S(E) = S_\delta \left[ 1 - \frac{iC(E)}{E - E_{\text{res}} + i\Gamma/2} \right], \quad (\text{B1})$$

where

$$S_\delta = \begin{pmatrix} 0 & e^{i\delta_L} \\ e^{i\delta_R} & 0 \end{pmatrix}$$

and

$$\begin{aligned} C(E) &= \frac{1}{i} (E - E_{\text{res}} + i\Gamma/2) \\ &\times (1 - S_\delta^{-1} \|f^{(+)}(E)\| \|f^{(-)}(E)\|^{-1}). \end{aligned}$$

The form (B1) is most convenient in the vicinity of the resonance energy  $E_r$ , where the  $S$  matrix is singular. If we assume that the resonances are isolated and correspond to simple zeros of the Jost matrix determinant, then near the point  $E_r$  the matrix function  $C(E)$  varies slowly and therefore can be approximated by  $C(E_r)$ , i.e.,

$$S(E) \approx S_\delta \left[ 1 - \frac{iC(E_r)}{E - E_{\text{res}} + i\Gamma/2} \right] (E \rightarrow E_r). \quad (\text{B2})$$

If  $E$  is real, the unitarity condition  $S^\dagger S = 1$  implies that

$$i(C^\dagger - C)(E - E_{\text{res}}) + C^\dagger C - (C^\dagger + C) \frac{\Gamma}{2} = 0.$$

This must be true for all  $E$  near  $E_{\text{res}}$ , which is only possible if  $C^\dagger = C$ . Therefore

$$[C(E_r)]^2 = \Gamma C(E_r). \quad (\text{B3})$$

Note that this cannot be reduced to  $C(E_r) = \Gamma$  because the inverse matrix  $C^{-1}(E_r)$  does not exist. Indeed,

$$\begin{aligned} C(E_r) &= iS_\delta^{-1} \lim_{E \rightarrow E_r} (E - E_r) \|f^{(+)}(E)\| \|f^{(-)}(E)\|^{-1} \\ &= \frac{i}{d} S_\delta^{-1} \|f^{(+)}(E)\| \|M\|, \end{aligned}$$

where  $d = \det ||f^{(-)}(E)|| / (E - E_r)$  and

$$||M|| = \text{cof}(|f^{(-)}(E_r)|) = \begin{pmatrix} f_{22}^{(-)} & -f_{12}^{(-)} \\ -f_{21}^{(-)} & f_{11}^{(-)} \end{pmatrix}$$

is the matrix made up of the cofactors of  $||f^{(-)}(E_r)||$  transposed. Since  $\det ||M|| = 0$  and therefore  $\det ||C(E_r)|| = 0$ , this implies that columns of  $C(E_r)$  are linearly dependent, i.e.,

$$C_{ll'}(E_r) = \gamma_l \eta_{l'},$$

where the choice of the numbers  $\gamma_l$  and  $\eta_{l'}$  is not unique. Using the fact that  $C^\dagger = C$ , we can choose them in such a way that

$$C_{ll'}(E_r) = \gamma_l \gamma_{l'}^*.$$

Then, from Eq. (B3), it follows that

$$\sum_l |\gamma_l|^2 = \Gamma. \quad (\text{B4})$$

Therefore, if we define  $\Gamma_L = |\gamma_L|^2$  and  $\Gamma_R = |\gamma_R|^2$ , then  $\Gamma = \Gamma_L + \Gamma_R$ .

It is easy to show that  $\Gamma_L$  and  $\Gamma_R$  determine the partial probabilities of decaying of the resonance into (or its exciting from) the left and right channels. Indeed, consider a wave packet

$$\psi_{\text{in}}(x, t) = \frac{1}{\sqrt{2\pi\hbar v_L^{\text{res}}}} \int_0^\infty e^{i(k_L x - Et/\hbar)} \omega(E) dE \quad (\text{B5})$$

that falls on the potential from the left with the average velocity  $\int_0^\infty \omega(E) v dE = v_L^{\text{res}}$  corresponding to the resonance energy  $E_{\text{res}}$ . We assume that the energy distribution  $\omega(E)$  has a narrow peak around this energy but this peak is wider than the resonance width  $\Gamma$ . Since the integrand in Eq. (B5) vanishes when  $E$  is far from  $E_{\text{res}}$ , we can extend the integration interval to  $(-\infty, +\infty)$ . This extension does not significantly affect its value but is convenient in the subsequent derivations. Then, according to Eq. (20), the scattered wave packet in the right channel is

$$\psi_{\text{out}}(x, t) = \frac{1}{\sqrt{2\pi\hbar v_R^{\text{res}}}} \int_{-\infty}^{+\infty} e^{i(k_R x - Et/\hbar)} S_{RL}(E) \omega(E) dE.$$

Expanding the function  $k_R(E)$  near the point  $E_{\text{res}}$ ,

$$k_R(E) \approx k_R^{\text{res}} + (E - E_{\text{res}}) \frac{dk_R}{dE} = k_R^{\text{res}} + \frac{E - E_{\text{res}}}{\hbar v_R^{\text{res}}},$$

we can approximate the corresponding probability density as

$$\begin{aligned} |\psi_{\text{out}}(x, t)|^2 &= \frac{\Gamma_L \Gamma_R}{2\pi\hbar v_R^{\text{res}}} \left| \int_{-\infty}^{+\infty} \frac{e^{i(k_R x - Et/\hbar)} \omega(E)}{E - E_{\text{res}} + i\Gamma/2} dE \right|^2 \\ &\approx \frac{\Gamma_L \Gamma_R |\omega(E_{\text{res}})|^2}{2\pi\hbar v_R^{\text{res}}} \\ &\quad \times \left| \int_{-\infty}^{+\infty} \frac{\exp\left[-\frac{i}{\hbar}(E - E_{\text{res}})(t - x/v_R^{\text{res}})\right]}{E - E_{\text{res}} + i\Gamma/2} dE \right|^2, \end{aligned}$$

where taking  $\omega(E)$  outside the integral is justified by the assumption that its peak is wider than  $\Gamma$ . The last integral can be evaluated by contour integration. This gives

$$\begin{aligned} |\psi_{\text{out}}(x, t)|^2 &= 2\pi \frac{\Gamma_L \Gamma_R |\omega(E_{\text{res}})|^2}{\hbar v_R^{\text{res}}} \\ &\quad \times \exp\left[-\frac{\Gamma}{\hbar}(t - x/v_R^{\text{res}})\right] \theta(t - x/v_R^{\text{res}}), \end{aligned}$$

where  $\theta(z)$  is the step function. The total probability  $P_R$  of seeing the particle in the right channel is then obtained by integrating  $|\psi_{\text{out}}(x, t)|^2$  over all  $x$ . The resulting value

$$P_R = 2\pi \frac{\Gamma_L \Gamma_R}{\Gamma} |\omega(E_{\text{res}})|^2$$

is factorized in the probability of capture the particle from the left channel  $P_{\text{capture}} = 2\pi\Gamma_L |\omega(E_{\text{res}})|^2$  and the probability that the resulting resonance decays into the right channel  $P_{\text{decay}} = \Gamma_R/\Gamma$ . Thus, the meaning of the quantities  $\Gamma_L$  and  $\Gamma_R$  becomes clear.

Equation (B2) offers a simple way of calculating the partial widths  $\Gamma_L$  and  $\Gamma_R$  as the limits

$$\Gamma_l = \lim_{E \rightarrow E_r} |(E - E_r) S_{ll}(E)|, \quad l = L, R.$$

In practical calculations, however, this procedure may cause numerical instabilities since the  $S$  matrix is singular at  $E = E_r$ . To avoid this difficulty, we can use the fact that the sum of the partial widths is already known,  $\Gamma_L + \Gamma_R = \Gamma$ . What remains is to find their ratio

$$\frac{\Gamma_L}{\Gamma_R} = \lim_{E \rightarrow E_r} \left| \frac{S_{LL}}{S_{RR}} \right|,$$

where the vanishing denominators of  $S_{LL}$  and  $S_{RR}$  (determinant of the Jost matrix) cancel out. Indeed, from Eqs. (19), (24), and (25) it follows that

$$\frac{\Gamma_L}{\Gamma_R} = \lim_{x \rightarrow \infty} \left| \frac{F_{1L}^{(-)}(E_r, -x) F_{2R}^{(-)}(E_r, x) - F_{1R}^{(-)}(E_r, x) F_{2L}^{(-)}(E_r, -x)}{F_{1L}^{(+)}(E_r, -x) F_{2R}^{(+)}(E_r, x) - F_{1R}^{(+)}(E_r, x) F_{2L}^{(+)}(E_r, -x)} \right|. \quad (\text{B6})$$

Therefore, the total width  $\Gamma$  is determined when we locate the resonance zero of the Jost matrix in the complex  $E$  plane. Then Eq. (B6) gives us the ratio  $\Gamma_L/\Gamma_R$  and the partial widths can be found from the condition  $\Gamma_L + \Gamma_R = \Gamma$ .

\*Email address: rakitsa@science.unisa.ac.za

<sup>1</sup>*Low-dimensional Semiconductor Structures*, edited by K. Barnham and D. Vvedensky (Cambridge University Press, Cambridge, 2001).

<sup>2</sup>L.R. Ram-Mohan, I. Vurgaftman, and J.R. Meyer, *Microelectron. J.* **30**, 1031 (1999).

<sup>3</sup>M. Steslicka, R. Kucharczyk, A. Akjouj, B. Djafari-Rouhani, L. Dobrzynski, and S.G. Davison, *Surf. Sci. Rep.* **47**, 93 (2002).

<sup>4</sup>S.D. Gunapala and S.V. Bandara, *Microelectron. J.* **30**, 1057 (1999).

<sup>5</sup>G. Strasser, P. Kruck, M. Helm, J.N. Heyman, L. Hvozdar, and E. Gornik, *Appl. Phys. Lett.* **71**, 2892 (1997).

<sup>6</sup>D. Bessis and G.A. Mezincescu, *Microelectron. J.* **30**, 953 (1999).

<sup>7</sup>E. Anemogiannis, E.N. Glytsis, and T.K. Gaylord, *Microelectron. J.* **30**, 935 (1999).

<sup>8</sup>E.J. Austin and M. Jaros, *Phys. Rev. B* **31**, 5569 (1985).

<sup>9</sup>V. V. Pupyshv and S. A. Rakityansky (unpublished).

<sup>10</sup>V.V. Pupyshv and S.A. Rakityansky, *Z. Phys. A* **348**, 227 (1994).

<sup>11</sup>S.A. Rakityansky, S.A. Sofianos, and K. Amos, *Nuovo Cimento Soc. Ital. Fis.*, **B 111**, 363 (1996).

<sup>12</sup>S.A. Sofianos and S.A. Rakityansky, *J. Phys. A* **30**, 3725 (1997).

<sup>13</sup>S.A. Rakityansky and S.A. Sofianos, *J. Phys. A* **31**, 5149 (1998).

<sup>14</sup>S.A. Rakityansky and S.A. Sofianos, *Few-Body Syst., Suppl.* **10**, 93 (1999).

<sup>15</sup>M. Bylicki, W. Jaskolski, and R. Oszwaldowski, *J. Phys.: Condens. Matter* **8**, 6393 (1996).

<sup>16</sup>W. Wasow, *Asymptotic Expansions for Ordinary Differential Equations* (Dover Publications, New York, 1987).

<sup>17</sup>J. Mathews and R. L. Walker, *Mathematical Methods of Physics* (W. A. Benjamin, New York, 1964).

<sup>18</sup>R. G. Newton, *Scattering Theory of Waves and Particles* (McGraw-Hill, New York, 1967).

<sup>19</sup>J. R. Taylor, *Scattering Theory* (John Wiley & Sons, New York, 1972).

<sup>20</sup>E. Merzbacher, *Quantum Mechanics* (John Wiley & Sons, New York, 1998).

<sup>21</sup>N. Imam, E.N. Glytsis, and T.K. Gaylord, *Superlattices Microstruct.* **29**, 411 (2001).

<sup>22</sup>M. V. Fedoryuk, *Asymptotic Analysis* (Springer-Verlag, Berlin, 1991).